

AD-A071 044

AEROSPACE CORP EL SEGUNDO CALIF AEROPHYSICS LAB
MEASUREMENTS OF ANOMALOUS DISPERSION OF HF IN ABSORPTION. (U)

F/G 7/4

UNCLASSIFIED

JUN 79 R W GROSS, R A CHODZKO, E B TURNER

F04701-78-C-0079

TR-0079(4764)-2

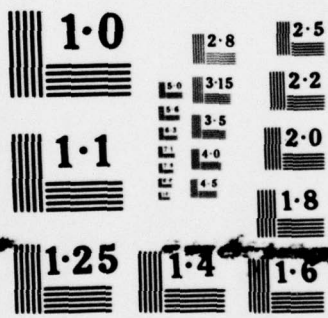
SAMSO-TR-79-44

NL

1 OF 1
AD
A071044



END
DATE
FILMED
8-79
DDC



NATIONAL BUREAU OF STANDARDS
MICROCOPY RESOLUTION TEST CHART

LEVEL II

①/2

AD A 071 044

**Measurements of the Anomalous
Dispersion of HF in Absorption**

R. W. F. GROSS, R. A. CHODZKO, E. B. TURNER, and J. G. COFFER
Aerophysics Laboratory
Laboratory Operations
The Aerospace Corporation
El Segundo, Calif. 90245

15 June 1979

Interim Report

DDC
REFILED
JUL 11 1979
REGISTERED
C

APPROVED FOR PUBLIC RELEASE;
DISTRIBUTION UNLIMITED

Sponsored by
DEFENSE ADVANCED RESEARCH PROJECTS AGENCY (DoD)
DARPA Order No. 3846
Monitored by SAMSO under Contract No. F04701-78-C-0079

SPACE AND MISSILE SYSTEMS ORGANIZATION
AIR FORCE SYSTEMS COMMAND
Los Angeles Air Force Station
P.O. Box 92960, Worldway Postal Center
Los Angeles, Calif. 90009

DDC FILE COPY

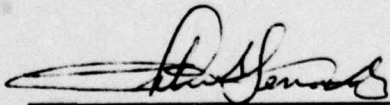
THE VIEWS AND CONCLUSIONS CONTAINED IN THIS DOCUMENT ARE THOSE
OF THE AUTHORS AND SHOULD NOT BE INTERPRETED AS NECESSARILY
REPRESENTING THE OFFICIAL POLICIES, EITHER EXPRESSED OR IMPLIED, OF
THE DEFENSE ADVANCED RESEARCH PROJECTS AGENCY OR THE U.S.
GOVERNMENT.

69 06 11 011

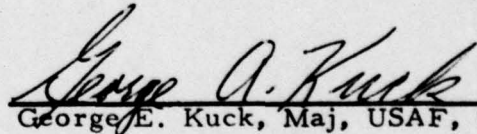
This interim report was submitted by The Aerospace Corporation, El Segundo, CA 90245, under Contract No. F04701-78-C-0079 with the Space and Missile Systems Organization, Deputy for Advanced Space Programs, P.O. Box 92960, Worldway Postal Center, Los Angeles, CA 90009. It was reviewed and approved for The Aerospace Corporation by W. R. Warren, Jr., Director, Aerophysics Laboratory, Lieutenant A. G. Fernandez, SAMSO/YCPT, was the project officer for Advanced Space Programs. Dr. H. Allan Pike is the Program Director for the DARPA Washington Office. This research was supported by the Defense Advanced Research Projects Agency of the Department of Defense.

This report has been reviewed by the Information Office (OI) and is releasable to the National Technical Information Service (NTIS). At NTIS, it will be available to the general public, including foreign nations.

This technical report has been reviewed and is approved for publication. Publication of this report does not constitute Air Force approval of the report's findings or conclusions. It is published only for the exchange and stimulation of ideas.



A. G. Fernandez, Lt, USAF
Project Officer



George E. Kuck, Maj, USAF, Chief
Technology Plans Division

FOR THE COMMANDER



FLOYD R. STUART, Colonel, USAF
Asst. Deputy for Technology

REPORT DOCUMENTATION PAGE		READ INSTRUCTIONS BEFORE COMPLETING FORM
1. REPORT NUMBER 18 SAMS0-TR-79-44	2. GOVT ACCESSION NO.	3. RECIPIENT'S CATALOG NUMBER
4. TITLE (and Subtitle) 6 MEASUREMENTS OF ANOMALOUS DISPERSION OF HF IN ABSORPTION	5. TYPE OF REPORT & PERIOD COVERED 9 Interim Rept.	6. PERFORMING ORG. REPORT NUMBER 14 TR-0079(4764)-2
7. AUTHOR(s) 10 Rolf W. F. Cross, Richard A. Chodzko, Eugene B. Turner, and John G. Coffey	8. CONTRACT OR GRANT NUMBER(s) 15 F04701-78-C-0079	10. PROGRAM ELEMENT, PROJECT, TASK AREA & WORK UNIT NUMBERS
9. PERFORMING ORGANIZATION NAME AND ADDRESS The Aerospace Corporation El Segundo, Calif. 90245	11. CONTROLLING OFFICE NAME AND ADDRESS Defense Advanced Research Projects Agency 1400 Wilson Blvd. Arlington, Va. 22209	12. REPORT DATE 11 15 June 1979
14. MONITORING AGENCY NAME & ADDRESS (if different from Controlling Office) Space and Missile Systems Organization Air Force Systems Command Los Angeles, Calif. 90009	13. NUMBER OF PAGES 51	15. SECURITY CLASS. (of this report) Unclassified
16. DISTRIBUTION STATEMENT (of this Report) Approved for public release; distribution unlimited	15a. DECLASSIFICATION/DOWNGRADING SCHEDULE	
17. DISTRIBUTION STATEMENT (of the abstract entered in Block 20, if different from Report)		
18. SUPPLEMENTARY NOTES		
19. KEY WORDS (Continue on reverse side if necessary and identify by block number) Absorption Anomalous Dispersion HF Experimental Measurements Infrared Mach-Zehnder Interferometer Vibrational Transitions		
20. ABSTRACT (Continue on reverse side if necessary and identify by block number) The quantitative measurement of the anomalous dispersion of the $P_1^{\uparrow}(6)$, $P_1^{\uparrow}(7)$, and $P_1^{\uparrow}(8)$ vibration-rotation transitions of hydrogen-fluoride (HF) in absorption are reported. The measurements were performed with a small, line-selectable HF laser equipped with a piezoelectrically frequency-scanned cavity that illuminated a Mach-Zehnder interferometer, one arm of which contained the HF absorption cell. The fringes produced by the interferometer and their dispersion-induced shift were observed directly with the help of a rotating mirror and an		

UNCLASSIFIED

SECURITY CLASSIFICATION OF THIS PAGE(When Data Entered)

19. KEY WORDS (Continued)

micron

20. ABSTRACT (Continued)

ir detector. This interferometer technique has an ultimate noise-limited sensitivity of 0.02 of a fringe spacing at 2.7 μm .

Measurements also are given for the absorption coefficient at line center for the same three P_1 lines of HF.

Both dispersion and absorption measurements are for a pressure range of 0.05 to 10 Torr of pure HF at room temperature, so the absorption lines were Doppler broadened. The measured values for the absorption coefficient and the slope of the dispersion curve at line center and for the maximum excursion of the anomalous refractive index are in excellent agreement with calculated values for these quantities.



UNCLASSIFIED

SECURITY CLASSIFICATION OF THIS PAGE(When Data Entered)

CONTENTS

I.	INTRODUCTION	7
II.	THEORETICAL CONSIDERATIONS	13
III.	EXPERIMENTAL APPARATUS.	19
	A. Optical Layout of Experiment	20
	B. Fringe Visualization Technique	23
IV.	EXPERIMENTAL RESULTS	27
	A. Frequency Jitter and Mode Pulling of Probe Laser	27
	B. Line-Scanned Absorption Measurements	36
	C. Measurements of Anomalous Refractive Index	38
V.	CONCLUSIONS	49

Accession For	
NTIS GRA&I	<input checked="" type="checkbox"/>
DDC TAB	<input type="checkbox"/>
Unannounced Justification	
By _____	
Distribution/	
Availability Codes	
Dist	Avail and/or special
A	

TABLES

1.	Calculated Values for Absorption Coefficient α_0 , Maximum Jump of Refractive Index $(1/P)\Delta(\eta - 1)_{JU}$, and Slope of Refractive Index Curve at Line Center $(1/P)(d\eta/d\nu)_{\nu_0}$ for Three Transitions.	17
2.	Measured Values and Standard Deviations of Absorption Coefficient α_0 , Slope of Anomalous Dispersion Curve $(1/P)(d\eta/d\nu)_{\nu_0}$ at Line Center, and Maximum Jump of Refractive Index $(1/P)\Delta(\eta - 1)_{JU}$ for Three HF Ground-State Transitions	17
3.	Oscilloscope Settings for Fringe Display	26
4.	Corrections for Free Spectral Scanning Range as Function of Mode Pulling for Various Cavity and HF Line Combinations of Probe Laser	32

FIGURES

1.	Line Profile and Anomalous Dispersion Curve for Doppler-Broadened Absorption Line	8
2.	Optical Layout of Experiment	21
3.	Electronic Fringe Scanning Equipment Schematic	24
4.	Gain Profile, Longitudinal Modes, and Power Output of the Scanning Probe Laser	28
5.	Frequency Jitter Measurement of Probe Laser Output	29
6.	Frequency Jitter of Probe Laser Output as Function of Observation Time Interval Δt	30
7.	Mode Pulling in Probe Laser	35
8.	Oscilloscope Record of Typical Intensity Scan of Absorption Line	37
9.	Measured Absorption Line Profiles of $P_1(7)$ for Three Different Combinations of Gas Pressure and Laser Scanning Range	39
10.	Absorption of Three HF Ground-State Transitions Measured at Line Center as Functions of Gas Pressure (Pure HF)	40
11.	Oscilloscope Trace of Typical Fringe Shift Measurement of $P_1(7)$	41
12.	Anomalous Dispersion Curve Derived from Experimental Record of Fig. 11	43
13.	Maximum Jump of Refractive Index Measured as a Function of Pressure in the Absorption Cell	45
14.	Slope of Anomalous Dispersion Curve at Line Center Measured as Function of Pressure in Absorption Cell	46

I. INTRODUCTION

The refractive index of the gain medium of a laser is an important optical parameter, especially if the index varies spatially and temporally throughout the medium. Such refractive inhomogeneities of the optical medium will distort the wave fronts, and, in the ultimate limit, destroy the coherence of the laser beam along with the beam quality. Gases have, under normal circumstances, a refractive index so close to one that index inhomogeneities can be neglected. However, in the vicinity of the lasing transitions themselves, the lasing medium exhibits an anomalous dispersion that results in non-negligible values of the refractive index. In addition, the refractive index changes drastically with frequency across the gain-line profile. Both of these effects may cause serious phase distortions in gas lasers if the density, the gain, and the length of the laser medium are large. In the cw HF(DF) chemical lasers of concern here, the situation may be aggravated even more by the simultaneous lasing of a large number of closely spaced vibration-rotation transitions that may influence each other.

The gain medium of an HF(DF) supersonic cw laser has a pressure of a few Torr, and the lasing transitions are Doppler broadened. The gain at the center of the line is of the order of a few percent per centimeter in these lasers. The transitions are dipole transitions, and the variation of the anomalous dispersion as a function of frequency can be calculated from standard theory.¹ A typical anomalous dispersion curve for an isolated, Doppler-broadened HF transition is shown in Fig. 1. As the frequency is changed away from line center in one direction, the refractive index increases to a maximum that is larger than one; in the opposite direction, it decreases to a minimum that is smaller than one. Near line center, the refractive index varies linearly with frequency. The two extrema occur at the frequency

¹

H. Mirels, Inhomogeneous Broadening Effects in CW Chemical Lasers, to be published in AIAA Journal.

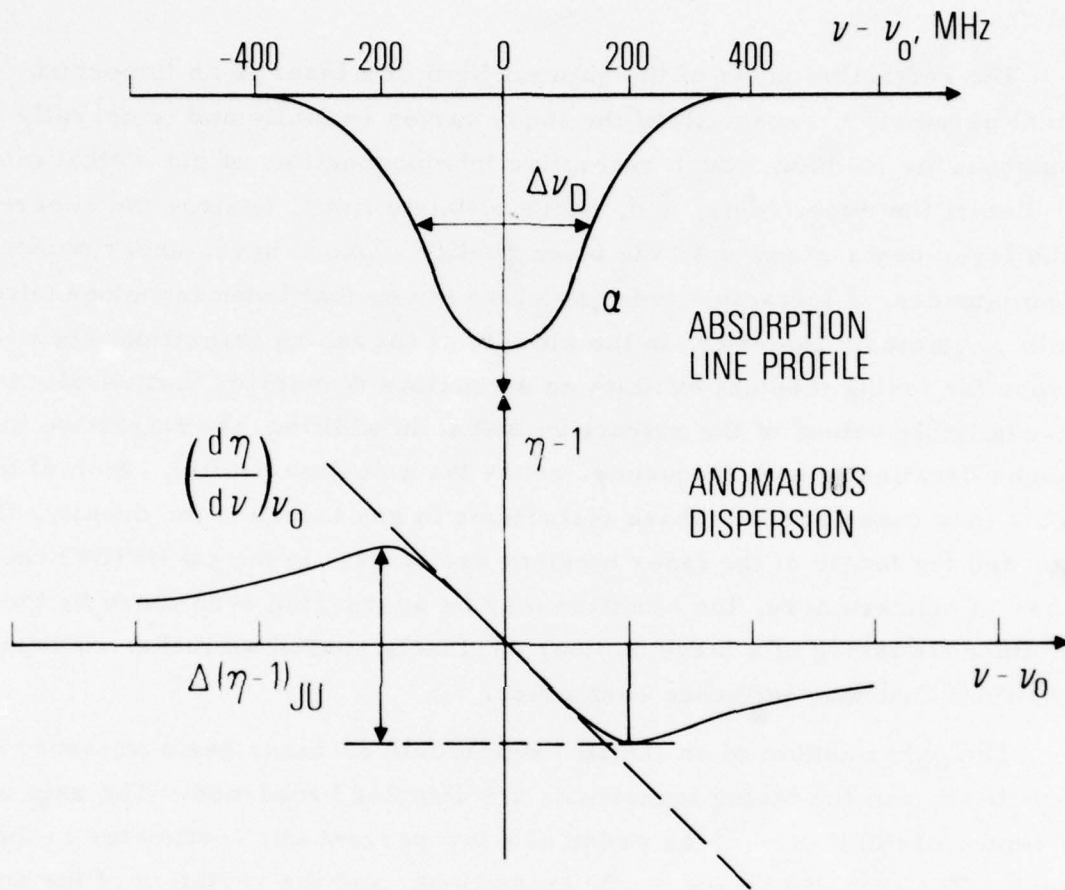


Fig. 1. Line Profile and Anomalous Dispersion Curve for Doppler-Broadened Absorption Line

where the gain or absorption profile reaches a value of $1/e$ of that at line center, that is, at points that are slightly outside the full Doppler width of the line. The magnitudes of the extrema and the slope of the index curve at line center are predicted to be proportional to the centerline gain or absorption coefficient.

This model applies only to an unsaturated-gain or absorption medium. When the medium is subjected to a high-power laser beam, the transition will be partly or fully saturated at the frequency where the laser mode interacts with the medium.¹ Since this medium is considered to be Doppler broadened, that is, inhomogeneously broadened, the laser beam or mode will burn a hole into the gain or absorption profile at the frequency of its interaction. The shape and width of the hole, which is homogeneously broadened, depends on the power in the laser mode and on the pressure-dependent relaxation processes active in the medium. If there are a large number of modes present, as is the case in long cavities of high-power HF chemical lasers, the interactions of the modes among each other and with the gain profile will affect the entire Doppler profile.¹ In turn, the complex saturation process will not only affect the gain profile but also the variation and magnitude of the anomalous dispersion. The index of refraction curve shown in Fig. 1 will be markedly distorted.

These questions have recently been investigated by Mirels¹ for a saturated HF chemical cw laser. Qualitatively, the entire gain profile can be depressed fairly uniformly in the laser medium by saturation and cross relaxation much as for an homogeneously broadened line, despite the fact that the line is not pressure broadened. Along with this reduction in gain, there is a reduction of the refractive index; phase distortions should, therefore, be small in a well-saturated HF laser.

The theoretical predictions of Mirels¹ so far have been experimentally verified only indirectly.*² The ultimate goal of the present investigation is

* R. A. Chodzko, The Aerospace Corporation, unpublished data.

² A. W. Anglebeck, Investigation of HF/DF Chemical Laser Physics, UTRC Report No. R76-912128-26, United Technologies Research Center, Hartford, Conn. (March 1976).

to measure the shape of the gain profile and the refractive index in the saturated medium of an HF laser directly and quantitatively. As a first step in this work, a highly sensitive interferometric technique was developed for measuring the refractive index, and the anomalous dispersion of three HF transitions in an unsaturated absorber. In this case, it is possible to calculate the refractive index from standard theory without dealing with the more complex problem of line saturation and to test and calibrate the experimental method against theory.

The anomalous dispersion was measured with a Mach-Zehnder interferometer illuminated by a single-line, single-mode, frequency-scanned, cw HF probe laser.³ The absorbing HF gas, contained in an absorption cell, was placed in one arm of the interferometer. As the probe laser was scanned in frequency across the absorption lines, the fringes produced by the interferometer shift position. Their shift is directly proportional to the refractive index of the absorber. A measurement of the fringe shift as a function of frequency will, therefore, provide a direct quantitative measurement of the anomalous refractive index in the vicinity of the absorption line. The maximum change of the refractive index and the slope of the anomalous dispersion curve at line center can be determined from a plot of the fringe shift versus frequency relationship.

Since these measurements are performed in absorption, three HF ground-state transitions, $P_1(6)$, $P_1(7)$, and $P_1(8)$, were investigated for a pressure range between 0.05 and 10 Torr of pure HF. In a separate series of experiments, the shape of these absorption lines and their absorption coefficient at line center were determined for the same pressure range. The measured values of these quantities were found to be in excellent agreement with those calculated from standard theory in the absence of saturation effects.

³D. J. Spencer, J. A. Beggs, and H. Mirels, "Small-Scale CW HF(DF) Chemical Laser," J. Appl. Phys. **48**, 1206 (1977).

Numerical calculations are presented that apply a basic theory to the three HF transitions in question. The lines were assumed to be Doppler broadened. The calculations are based on the recent review by Mirels.¹ A detailed description of the experimental equipment and its use in our measurements is also given. Our experience and that of others* indicate that the stability of the probe laser plays a crucial role in such measurements. Therefore, detailed information concerning the probe laser is given, and how its inherent instability can be eliminated from influencing the experiments is discussed. It was also found that the probe laser is subject to extensive mode pulling when it is frequency scanned. In addition, the experimental results are compared with the numerical predictions.

*A. W. Anglebeck, private communication.

II. THEORETICAL CONSIDERATIONS

A weak laser beam probing a Doppler-broadened absorption line experiences a frequency-dependent anomalous refractive index $\eta(\nu)$. Mirels¹ has recently reviewed the theory describing this interaction for the case of a chemical laser, which also applies to a low-pressure HF absorbing gas. Mirels expresses the refractive index as

$$\eta(\nu) - 1 = \frac{\lambda_0}{\sqrt{\pi}} \frac{1}{4} \sigma_0 \bar{p}_0 \Delta\nu_H (n_2 - n_1) D(x) \quad (1)$$

where

$$D(x) = e^{-x^2} \int_0^x e^{\xi^2} d\xi = \text{the tabulated Dawson Integral}^4$$

$$x = (4 \ln 2)^{1/2} (\nu - \nu_0) / \Delta\nu_D$$

λ_0 = center wavelength of absorption line (cm)

ν_0 = center frequency of absorption line (Hz)

σ_0 = absorption cross section of the homogeneous line (cm²) at line center

$\Delta\nu_H$ = full width at half maximum of the homogeneous line (Hz)

$\Delta\nu_D$ = full width at half maximum of the Doppler line (Hz)

\bar{p}_0 = Boltzmann distribution function (sec)

n_1, n_2 = densities of the lower and upper excited states (cm⁻³)

Then,

$$\sigma_0 \bar{p}_0 \Delta\nu_H (n_2 - n_1) = \frac{2}{\pi} \sigma_{\nu} J(n_2 - n_1) \quad (2)$$

⁴M. Abramowitz and I. A. Stegun, eds., Handbook of Mathematical Functions, U.S. Government Printing Office, Washington, D.C. (1966).

and, by definition of α_0 ,

$$\sigma_0 \bar{P}_0 \Delta \nu_H (n_2 - n_1) = \frac{2}{\pi} \alpha_0 P \quad (2b)$$

where

$\sigma_{v, J}$ = vibration-rotational absorption cross section (cm^2)

α_0 = absorption coefficient (cm Torr^{-1}) at line center

P = total pressure of the absorbing gas (Torr)

Therefore, for the refractive index as a function of frequency,

$$\eta(\nu) - 1 = \frac{\lambda_0}{2\pi} \frac{3/2}{\alpha_0 P D(x)} \quad (3)$$

The variation of the index of refraction is shown as a function of frequency in Fig. 1 along with the absorption of the line. From the fringe shift experiments, two quantities can be determined, the slope of the index of refraction curve at line center and the maximum change of the index, that is, the absolute sum of the magnitude of the maximum and minimum of the index curve.

The maximum and minimum of the Dawson integral occurs for $x \approx \pm 0.92$; the distance between the extrema is, therefore,

$$2|\nu_m - \nu_0| \approx \frac{0.92 \Delta \nu_D}{(\ln 2)^{1/2}} \approx 1.12 \Delta \nu_D \quad (4)$$

where for HF,

$$\Delta \nu_D = 4.803 \times 10^3 \frac{1}{\lambda} \sqrt{T} \text{ (Hz)}$$

The value for the Dawson integral at the extrema is

$$D(\pm 1) = \pm 0.5381$$

and the absolute sum of the maximum and minimum of the index curve, the maximum index jump $\Delta(\eta - 1)_{JU}$, is

$$\frac{1}{P} \Delta(\eta - 1)_{JU} = \frac{0.5381 \lambda_0}{\pi^{3/2}} \alpha_0 = 0.1047 \lambda_0 \alpha_0 (\text{Torr})^{-1} \quad (5)$$

The slope of the index curve at line center $(d\eta/d\nu)_{\nu = \nu_0}$ is easily obtained by differentiation of Eq. (3)

$$\left[\frac{d\eta}{d\nu} \right]_{\nu_0} = \frac{(\ln 2)^{1/2} \alpha_0 \lambda_0 P}{\pi^{3/2} \Delta\nu_D} [D'(x)]_0 \quad (6)$$

The slope of the Dawson integral at $x = 0$ is 1,

$$[D'(x)]_0 = 1$$

Therefore,

$$\begin{aligned} \frac{1}{P} \left[\frac{d\eta}{d\nu} \right]_{\nu_0} &= \frac{(\ln 2)^{1/2} \alpha_0 \lambda_0}{\pi^{3/2} \Delta\nu_D} (\text{Torr Hz})^{-1} \\ &= 0.1495 \frac{\alpha_0 \lambda_0}{\Delta\nu_D} \end{aligned} \quad (7)$$

For a Doppler-broadened line, the separation of the extrema of the anomalous dispersion curve is slightly larger than the full width of the Doppler

line and is independent of pressure. The maximum jump of the index of refraction and the slope of the dispersion curve at line center are, however, proportional to pressure and the absorption coefficient at line center. Values for these quantities, calculated from the above expressions for the three transitions of our measurements and a temperature of $T = 297$ K, are given in Table 1. The values for the absorption coefficients were provided by Hough^{*} and were calculated with the use of the dipole matrix elements of Meredith.⁵

The magnitude of these quantities is evident when they are compared to the average refractive index of HF and He, two gases that play an important part in HF cw lasers, far away from any resonance lines. At 1 Torr and 297 K, the refractive index of HF calculated from its molecular polarization is $n_{\text{HF}} - 1 = 9.8 \times 10^{-7}$, and for He $n_{\text{He}} - 1 = 8.4 \times 10^{-8}$, the magnitude of the anomalous index of refraction near the HF transitions is one to two orders of magnitude larger and dominates the refractive index in this part of the spectrum (Table 2).

* J. J. Hough, The Aerospace Corporation, private communication.

⁵ R. E. Meredith and F. G. Smith, J. Quantum Spectroscopy and Radiative Transfer **13**, 89 (1973).

Table 1. Calculated Values for Absorption Coefficient α_0 , Maximum Jump of Refractive Index $(1/P)\Delta(\eta - 1)_{JU}$, and Slope of Refractive Index Curve at Line Center $(1/P)[d\eta/d\nu]_{\nu_0}$ for Three Transitions. Temperature of Absorbing Gas $T = 297$ K.

Line	λ_0 , μm	α_0 , $(\text{Torr cm})^{-1}$	$\frac{1}{P} \Delta(\eta - 1)_{JU}$, Torr^{-1}	$\frac{1}{P} \left[\frac{d\eta}{d\nu} \right]_{\nu_0}$, $(\text{Torr MHz})^{-1}$
$P_1(6)$	2.707	0.499	1.41×10^{-5}	6.60×10^{-8}
$P_1(7)$	2.744	0.152	4.36×10^{-6}	2.06×10^{-8}
$P_1(8)$	2.783	0.038	1.11×10^{-6}	5.32×10^{-9}

Table 2. Measured Values and Standard Deviations of Absorption Coefficient α_0 , Slope of Anomalous Dispersion Curve $(1/P)(d\eta/d\nu)_{\nu_0}$ at Line Center, and Maximum Jump of Refractive Index $(1/P)\Delta(\eta - 1)_{JU}$ for Three HF Ground-State Transitions. Temperature of Absorbing Gas $T = 297$ K.

Line	α_0 , $(\text{Torr cm})^{-1}$	$\frac{1}{P} \Delta(\eta - 1)_{JU}$, Torr^{-1}	$\frac{1}{P} \left[\frac{d\eta}{d\nu} \right]_{\nu_0}$, $(\text{Torr MHz})^{-1}$
$P_1(6)$	0.51 ± 0.04	$(1.53 \pm 0.26) \times 10^{-5}$	$(7.48 \pm 1.34) \times 10^{-8}$
$P_1(7)$	0.15 ± 0.02	$(5.04 \pm 1.2) \times 10^{-6}$	$(2.19 \pm 0.55) \times 10^{-8}$
$P_1(8)$	0.038 ± 0.006	$(1.33 \pm 0.34) \times 10^{-6}$	$(5.05 \pm 1.17) \times 10^{-9}$

III. EXPERIMENTAL APPARATUS

The anomalous dispersion of resonance transitions in the visible part of the spectrum is classically determined by the so-called "Hook Method" developed by Rozhdestvenskii⁶ and others.⁷ In this technique, a Mach-Zehnder interferometer is used, which has the medium in one arm of the interferometer and an incoherent continuous light source for illumination. The output of the interferometer is viewed by a spectrograph, the entrance slit of which is arranged perpendicular to the fringes produced by the interferometer. A photographic record in the spectrograph exit plane shows the fringes crossing the absorption lines of the medium. Because of the changing anomalous dispersion of the absorber, the fringes are distorted on both sides of the absorption lines and form two "hooks" that correspond to the two extrema of the dispersion curve.

Unfortunately, this elegant method is not suitable for measurements in the infrared: there are no photographic plates available to record the two-dimensional field of crossed fringes and absorption lines, and there are no continuous light sources of sufficient strength in this part of the spectrum. The interferometric technique is still the most direct way of measuring the refractive index of a medium, and the problem to be faced experimentally is primarily that of finding a method of recording the two-dimensional field in fringe shifts versus frequency. The problem of a powerful light source and of a spectroscopic instrument of sufficiently high resolution can be solved with the aid of a tunable laser.

With the use of a tunable laser and an interferometer, the fringe shifts have been investigated previously with a phase-sensitive heterodyne

⁶D. S. Rozhdestvenskii and N. P. Penkin, J. Phys. USSR 5-6, 319 (1941).

⁷For a general review, see B. Bederson and W. L. Fite, Methods of Experimental Physics, Volume 7-A: Atomic Interactions, Academic Press, N.Y. (1968) p. 127.

technique.⁸ This method requires a second, frequency-stabilized laser as a local oscillator in addition to other sophisticated electronic equipment. The simpler and more direct way of scanning the fringes with a fast mechanical scanning mirror was used here. This method can be made to be very sensitive. It also permits fast single scans to be made of the fringes in real time, circumventing the problems introduced by the poor frequency stability of the tunable laser.

A. OPTICAL LAYOUT OF EXPERIMENT

The layout of the optical equipment is shown in Fig. 2. A small, electrically driven HF cw-laser serves as the tunable laser light source. This laser has been described elsewhere.⁸ It could be interchangeably equipped with a medium of either 10 or 15 cm length l . The laser cavity consists of a grating with 300 lines/mm and a concave mirror of 125 cm radius mounted on a piezoelectric transducer. Three different cavity lengths L , 37.5, 30, and 27.5 cm, were used to obtain different mode separations and different free-spectral scanning ranges. Two apertures in the cavity restricted the laser to the TEM_{00} mode. The grating was tuned to the desired HF line and a spectrograph, not shown in Fig. 2, could be inserted into the optical path to determine the lasing line. In the scanning mode, the laser typically produced an average power of 150 mW on any of the three P_1 lines used in these experiments.

The output beam of the laser passed through a number of beam-steering mirrors and was then enlarged eight times to a diameter of 3.0 cm by a beam-expanding telescope assembled from a CaF_2 lens with a focal length f of 15 cm and a concave mirror of radius $R = 240$ cm. The telescope was arranged such that the beam left the exit mirror parallel.

This system illuminated a Mach-Zehnder interferometer constructed of two beam-splitter plates (SP1 and SP2) and two plane mirrors (M1 and M2)

⁸A. W. Anglebeck, UTRC Report No. R76-912128-26, United Technologies Research Center, Hartford, Conn. (March 1976).

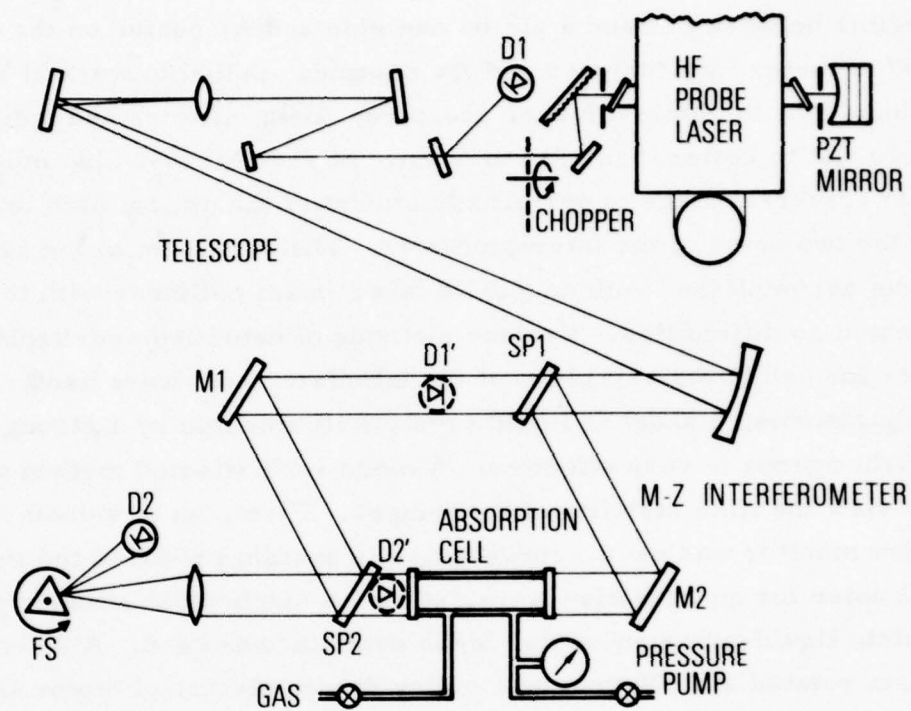


Fig. 2. Optical Layout of Experiment

mounted in 10-cm-diameter precision gimbals. The splitter plates were 7.5-cm-diameter Zn-Se plates coated to a reflectivity of 50% in the wavelength regime between 2.7 and 4 μm on one side and Ar coated on the other. The interferometer was designed and the coatings applied to work at a 30-deg angle of incidence to obtain a larger aperture. Both mirrors and splitter plates were flat to better than $\lambda/15$ at 3 μm . Mirror M1 was also mounted on a linear traversal stage to permit adjustment of the optical path lengths of one of the two arms of the interferometer. The alignment of the interferometer was accomplished with an He-Ne laser beam collinear with the ir beam and presented no difficulties. Various methods of detecting and displaying the fringes formed in the exit plane of the interferometer were used. For simple adjustments, a sheet of liquid crystals illuminated by a strong incandescent light source is very effective. A more sophisticated method was needed to view the time stability of the fringes. First, an ir vidicon with a television monitor was used. However, this system produced too much electrical noise for quantitative work, so that a mechanical scanner and a single-point, liquid-nitrogen-cooled In-Sb detector was used. A Au-coated glass prism rotated at 2800 rpm by a pulley driven electrical motor was used as a scanner. A lens placed in front of the scanner was used to adjust the magnification of the fringe pattern on the detector aperture. The interferometer was adjusted such that the fringes were perpendicular to the scanning direction.

Two absorption cells were used in the experiments, a long cell of 46.3 cm and a short cell of 5.08 cm length. Both cells had an inner diameter of 2.5 cm and were equipped with an interferometrically matched pair of CaF_2 windows. HF gas could be flowed through the cells from a small tank. The gas pressure in the cell was measured with a capacitance manometer. A diffusion pump permitted the evacuation of the cell to pressures of the order of 10^{-5} Torr. After an initial passivation, the HF gas in the cells disappeared, only very slowly by wall reaction, so that most experiments could be performed with a static filling of the gas.

During the interferometric measurements a second liquid-nitrogen-cooled In-Sb detector, D1, was inserted into the laser beam near the laser exit mirror to monitor the laser output power.

For the line-scanned absorption measurements, the two detectors were moved into the two interferometer arms, to positions D1' and D2' (Fig. 2). In these experiments, scatter plates were placed in front of the apertures of both detectors to ensure an integrated measurement over the beam area. The beam was interrupted with a fast chopper to produce a controlled zero-power reference for the absorption measurements.

All the optical equipment except for the HF laser body, its discharge tubes, and pump lines was placed on an air-suspended optical table. The laser was mounted on a separate stand that cantilevered over the table. This arrangement effectively separated the pump vibrations from the sensitive interferometer. It was also found necessary to protect the interferometer by a large box from air currents.

B. FRINGE VISUALIZATION TECHNIQUE

In the final experiments, the interferometer fringes were viewed by a rotating mirror scanner and a single-point, liquid-nitrogen-cooled In-Sb detector in the exit plane of the interferometer. The three-sided rotating mirror was running freely at 2800 rpm, scanning the entire fringe pattern, perpendicular to the fringes, in about 100 μ sec with a repetition rate of one scan every 7.14 msec. A transducer attached to the rotating mirror produced voltage pulses that were synchronized with the faces of the mirror. These pulses were used to trigger an oscilloscope (OSC1 in Fig. 3) and also to define the time position of the mirror scan by displaying them on oscilloscope OSC1, which was swept at 10 msec/div.

The sawtooth voltage of oscilloscope OSC1 was amplified by a high-voltage amplifier (Burleigh HV-70) and then used to drive the PZT mirror of the probe laser cavity. The amplification of the high-voltage amplifier was adjusted such that the laser was swept through one free spectral range during

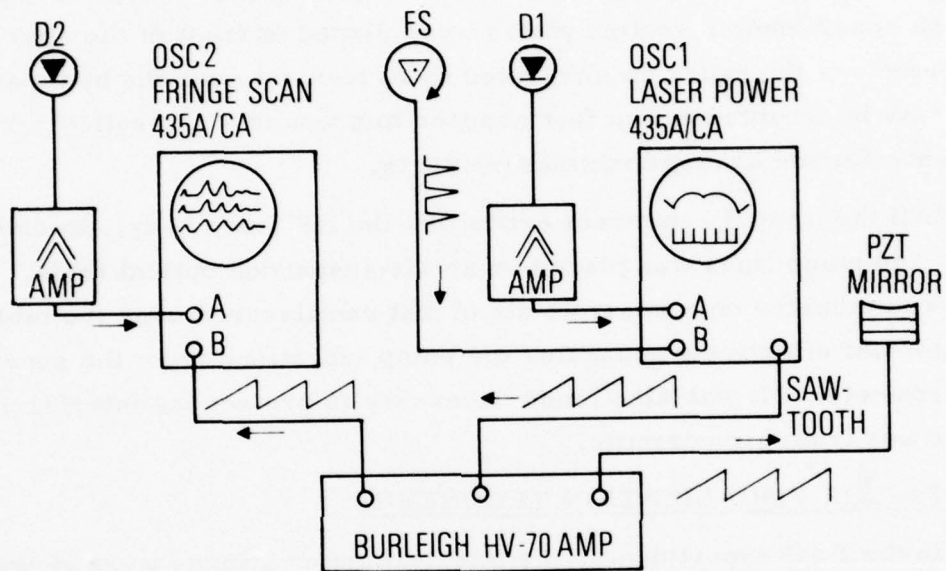


Fig. 3. Electronic Fringe Scanning Equipment Schematic

one sweep of oscilloscope OSC1. A room-temperature In-As detector, also displayed on oscilloscope OSC1, monitored the power output from the laser. Two strong dips in the laser power output marked the jump from one cavity mode to the next one. The distance between the power dips is a measure of the effective free spectral range of the laser. By means of the bias offset voltage of the high-voltage amplifier, the laser power sweep could be manually centered with respect to the sweep of oscilloscope OSC1.

A second output of the high-voltage amplifier, producing a voltage of 1/100 of the PZT driver voltage, was fed to one channel of the dual-channel amplifier of a second oscilloscope (OSC2 in Fig. 3). There it was added to the signal derived from detector D2, which viewed the fringe pattern behind the rotating mirror.

When both oscilloscopes are run at the same sweep speed of 10 msec/div, a steep ramp function with fourteen 100- μ sec spikes produced by the fringe scan detector, D2, is seen on oscilloscope OSC2. If the sweep of Oscilloscope 2 is reduced to 20 μ sec/div and oscilloscope OSC2 is triggered internally by the "marker" signals preceding each fringe scan, all of the 14 fringe scans made by the rotating mirror during one laser sweep can be made to appear simultaneously on the face of oscilloscope OSC2. The scans are displayed vertical from each other by the PZT ramp voltage. In Fig. 11a, which will be discussed in detail later, a typical fringe scan obtained in this way is shown. For future reference and to increase the clarity of this discussion, the relevant settings of the two oscilloscopes are given in Table 3.

The signals from the two detectors were amplified 30 times by two identical dc amplifiers with a bandwidth of about 30 kHz before displaying them on the oscilloscopes.

Table 3. Oscilloscope Settings for Fringe Display

	TRIGGER	PREAMPLIFIER	TIME BASE A
Oscilloscope OSC2, 435A	AC, INT Level = + Slope = +	Type CA, Mode = CHOP Channel A = 0.5 V/cm AC, CAL Channel B = 2 V/cm AC, CAL	SINGLE SWEEP or NORMAL, 10 msec/cm, UNCAL
Oscilloscope OSC1, 435A	AC, INT Level = + Slope = +	Type CA, Mode = ADD Channel A = IV/cm AC, CAL Channel B = 0.5 V/cm DC, UNCAL	NORMAL, 20 μ sec/cm, CAL

IV. EXPERIMENTAL RESULTS

A. FREQUENCY JITTER AND MODE PULLING OF PROBE LASER

Two properties (Fig. 4) of the scanning probe-laser strongly influence its use as a light source in these experiments: (1) the laser mode is subject to a sizable frequency jitter caused by mechanical vibrations of the mirror mounts and (2) when scanning the mode across the gain-line, mode pulling strongly reduces the separation between the modes and therefore the available scanning range of the cavity. The gain profile of a single laser line and four of the longitudinal cavity modes are shown in Fig. 4. The nominal free spectral range, which is equal to the mode spacing, was made large by making the cavity length L short to ensure that only one mode is capable of lasing under the given gain profile. Varying the cavity length by scanning one of the cavity mirrors moves the modes across the gain line. The same thing happens as a result of the statistical variations of the mirror spacing of the cavity, which causes frequency jitter.

The frequency jitter of the cavity was investigated experimentally. The laser was tuned to the desired line, and its output scanned with a confocal etalon. The 25-cm-long, 300-MHz cavity of the confocal etalon was scanned with the aid of a PZT driven by the amplified sawtooth voltage of an oscilloscope. The same oscilloscope was then used to display the signal from a fast detector that looked at the radiation transmitted by the etalon. Two resonances were observed, separated by the 300-MHz free spectral range of the confocal etalon. The frequency jitter of the resonance peaks corresponds to that of the laser cavity. The etalon was scanned through its free spectral range once every 10 msec. The jitter was observed by opening the oscilloscope camera for various time durations Δt (Fig. 5). The full width at half maximum $\Delta\nu$ of the jitter pattern, corrected for the FWHM of the etalon of 28 MHz, is plotted for the nominally 500-MHz cavity of the laser as a function of the observation time interval in Fig. 6. Each point in Fig. 6 corresponds to the average of 10 separate measurements. The frequency jitter increases

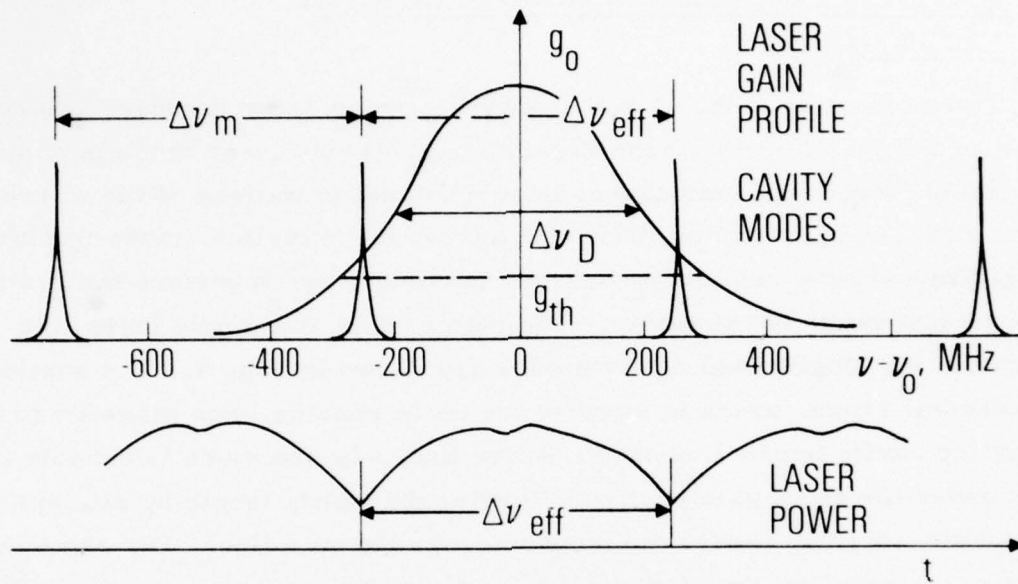
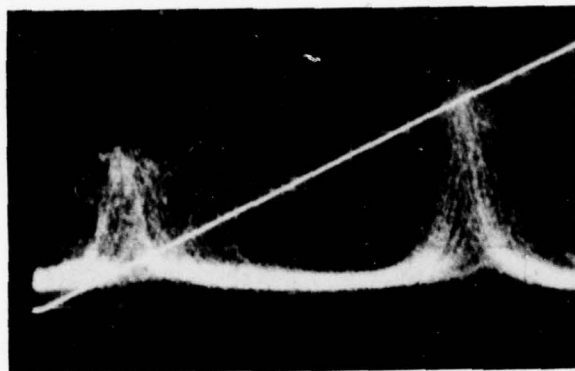
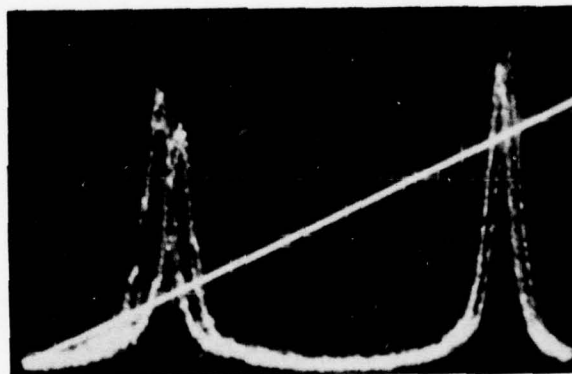


Fig. 4. Gain Profile, Longitudinal Modes, and Power Output of Scanning Probe Laser



(a)



(b)

Fig. 5. Frequency Jitter Measurement of Probe Laser Output. Single-line operation on $P_1(7)$. Effective free spectral range of laser cavity = -458 MHz. Free spectral scanning range of confocal analyzer etalon = 300 MHz. (a) 2-sec observation time. (b) 0.1-sec observation time.

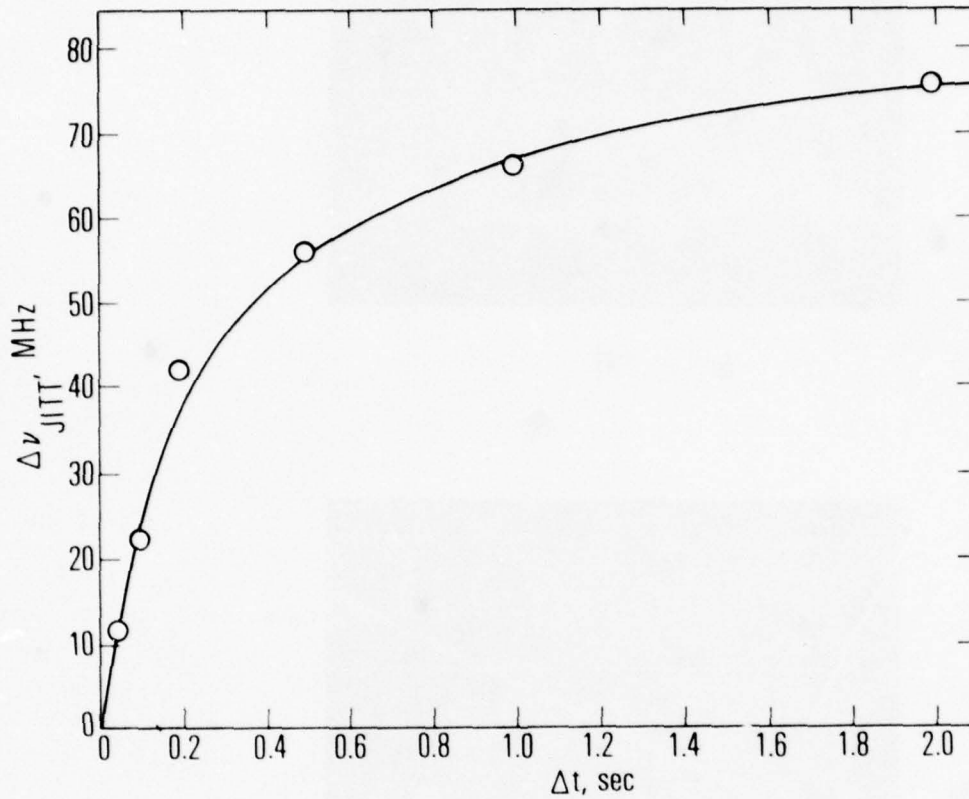


Fig. 6. Frequency Jitter of Probe Laser Output as Function of Observation Time Interval Δt . Single-line operation on $P_1(7)$. Effective free spectral range of laser cavity = 458 MHz. Free spectral scanning range of confocal analyzer etalon = 300 MHz. Each point is average of 10 observations.

rapidly with increasing observation time and finally reaches a constant relatively large value for large times. This asymptotic value is defined by the mechanical construction of the cavity and the finite width of the gain profile of the laser medium. The time interval during which the laser radiation is viewed had to be reduced to make the frequency jitter a small fraction of the free spectral range. In the interferometer experiments, this time interval is the time the PZT mirror in the laser cavity takes to scan the gain width of the gain line. One hundred milliseconds was chosen as the time interval. In the present experiments, this scanning time is limited by the speed of the rotating mirror sweeping the fringes and the number of fringe scans desired during one cavity scan. With a higher rotational speed of the mirror, it would be possible to decrease the cavity scan time to 10 msec, the response limit of the PZT driver, and still be able to sample the fringe pattern 20 times during each cavity scan.

Figure 6 indicates that the frequency jitter during a 100-msec viewing time is on the average 22 MHz, which results in a statistical scatter of the frequency measurement in the fringe experiments of $22/500 = 5\%$ of the nominal free spectral range of the laser cavity.

There is also a slow drift of the probe laser cavity as a result of thermal expansion, slow variations of the gain medium, and drifts of the optical table. This frequency drift was corrected for manually by adjusting the PZT offset bias voltage on the scanning mirror.

The laser cavity should be as short as possible to obtain a large scanning range of the probe laser. The shortest cavity length achieved was limited by the width of the flow duct containing the laser medium. The combinations of cavity lengths L and medium lengths l used in the experiments are given in Table 4. The medium fills a sizable portion of the cavity, and for such cavities, large mode-pulling effects have to be expected.

Frequency pulling of the laser cavity modes is a consequence of the anomalous refractive index of the gain medium. Modes that do not coincide

Table 4. Corrections for Free Spectral Scanning Range as Function of Mode Pulling for Various Cavity and HF Line Combinations of Probe Laser. $T = 400$ K.

l , cm	L , cm	$\Delta \nu$, m' MHz	$P_1(6)$			$P_1(7)$			$P_1(8)$					
			x_m	β	$\Delta \nu_{eff}$, MHz	x_m	β	$\Delta \nu_{eff}$, MHz	x_m	β	$\Delta \nu_{eff}$, MHz			
15	37.5	400				0.95	0.154	364						
15	30.0	500	1.17	0.189	456	1.19	0.192	458	1.19	0.195	449			
10	25.7	583				1.38	0.149	551	1.38	0.152	540			
		$\Delta \nu_D$, MHz						355			351			344

with the center ν_0 of the gain line are pulled from their empty cavity position ν_m to a frequency ν_{eff} that is closer to line center, which results in a reduction of the free spectral range of an empty cavity $\Delta\nu_m = c/2L$ to an effective free spectral range $\Delta\nu_{\text{eff}}$ and in a distortion of the linear relationship between ν_{eff} and the driving voltage of the scanning PZT.

Mode pulling can be measured experimentally by comparing the frequency of the scanned laser cavity to a frequency reference, for example, a second stabilized HF laser. Instead, it was decided to correct the experiments for mode pulling numerically. This simpler procedure will be justified later by comparing the measured Doppler line shapes with calculated line shapes.

The theory of mode pulling has been investigated by several authors.⁹ Since the medium of the low-power subsonic, HF probe-laser under these experimental conditions is Doppler broadened and only weakly saturated (the laser was operated at about 1/10 of its maximum single line output), the simple theory given by Casperson and Yariv¹⁰ should apply.

Casperson and Yariv derived a relationship between the empty cavity mode separation $\Delta\nu_m$ and the effective separation $\Delta\nu_{\text{eff}}$. In nondimensional form

$$x_m - x_{\text{eff}} = \beta D(x_{\text{eff}}) \quad (8)$$

where

$$x_m = \frac{(\ln 2)^{1/2}}{\Delta\nu_D} \Delta\nu_m, \quad x_{\text{eff}} = \frac{(\ln 2)^{1/2}}{\Delta\nu_D} \Delta\nu_{\text{eff}} \quad (9)$$

⁹D. H. Close, Phys. Rev. **153**, 360 (1967).

¹⁰L. Casperson and A. Yariv, Appl. Phys. Lett. **17**, 259 (1970).

and

$$\beta = \frac{\ell}{L} \frac{cg_0(\ln 2)^{1/2}}{\pi^{3/2} \Delta\nu_D} \quad (10)$$

$D(x_{\text{eff}})$, the Dawson integral, $\Delta\nu_m$, $\Delta\nu_{\text{eff}}$, L , ℓ , and $\Delta\nu_D$ have all been defined previously. g_0 is the small-signal-gain coefficient at line center.

The implicit relationship, Eq. (8), for x_{eff} is obviously closely related to the expression for the refractive index of a Doppler-broadened line given earlier. The Dawson integral can be approximated by $D(x_{\text{eff}}) \approx x_{\text{eff}}$ for small values of x_{eff} , which results in an explicit relationship for x_{eff} and, hence, $\Delta\nu_{\text{eff}}$

$$x_{\text{eff}} \approx \frac{x_m}{1 + \beta}, \quad \Delta\nu_{\text{eff}} \approx \frac{\Delta\nu_m}{1 + \beta} \quad (11)$$

which indicates that the empty-cavity free spectral range is reduced by a factor $1/(1 + \beta)$ when the gain medium is introduced into the cavity. At the same time, the slope of the relationship between x_{eff} , the effective mode frequency, and x_m , the nominal frequency related to the driving voltage of the scanning PZT, is reduced by the same factor. The effective mode frequency x_{eff} varies linearly, however, with the driving voltage.

Values for x_m and β for the three cavities of the experiments are given in Table 4. Since the frequency excursions scan a sizable portion of the gain-line width and x_{eff} is not small, Eq. (8) has been solved numerically. The values for the effective mode separation and, therefore, the effective free spectral scanning range obtained in this way are also given in Table 4 for the three cavity configurations and the three HF lines used in these experiments. The deviation of the movement of the mode in the medium compared to that of the empty cavity and the linearized prediction according to Eq. (11) for one specific configuration is shown in Fig. 7.

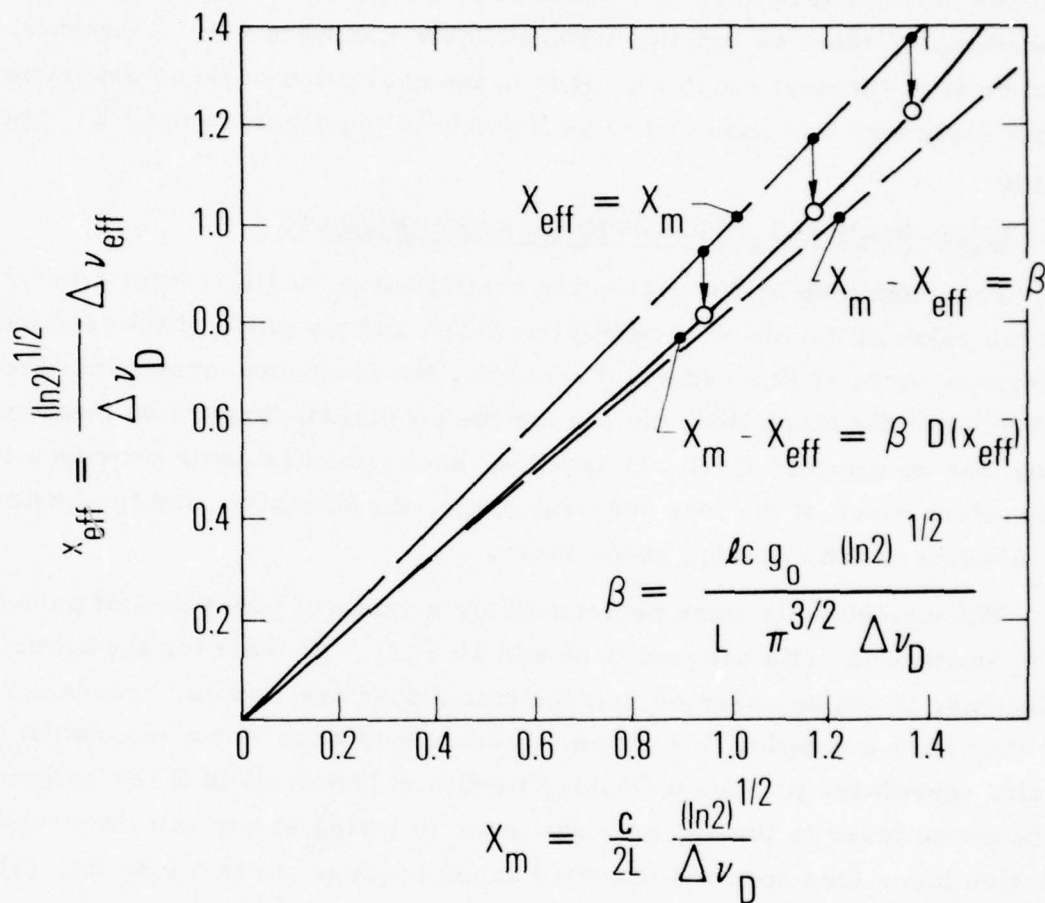


Fig. 7. Mode Pulling in Probe Laser. x_m is nondimensional, nominal free spectral range of the laser cavity. x_{eff} is nondimensional, effective free spectral range produced by mode pulling effects. Three points correspond to three cavity configurations of experiments.

Whereas the free scanning range is reduced sizably in these experiments, the mode movement is still very close to a straight line in frequency and proportional to the PZT driving voltage (Table 4 and Fig. 7). Therefore, the effective free spectral range was used in the evaluation of these experiments, but the frequency was assumed to be linearly proportional to the PZT driver voltage.

B. LINE-SCANNED ABSORPTION MEASUREMENTS

The magnitude of the absorption coefficient α_0 at line center determines both the value of the absolute refractive index and the slope of the anomalous dispersion curve at line center. Therefore, the frequency-dependent absorption coefficient of the three lines chosen for the anomalous dispersion measurements was determined first. In addition, such measurements provide a simple independent check of the free spectral range, the linearity, and the mode jumping behavior of the scanning probe laser.

The experiments were performed for a range of pressures of pure HF in the absorption cells between 0.05 and 10 Torr. At least for the lower pressures, it can be assumed that the transitions are Doppler broadened and that they have a Doppler line shape. A frequency scan of the absorption line should, therefore, provide a Doppler profile of known width if the scanning of the probe laser is linear, only one mode is lasing at any one time, and the effective laser free spectral scanning range is given correctly by Eq. (8).

A typical record of an absorption measurement of the HF $P_1(7)$ line is given in Fig. 8. The upper trace is the signal I_0 , seen by detector D1', which is proportional to the power output of the probe laser before entering the cell. The lower trace is I , the power of the laser beam after it passed the absorption cell as seen by detector D2'. Both signals were equal in shape and amplitude when no HF gas was in the cell. A small Lamb dip can be seen in the center of I_0 . The effective free spectral range calculated for this experiment was $\Delta\nu_{\text{eff}} = 458$ MHz, corresponding to the shortest cavity listed in Table 4 and the 10-cm-long medium. The pressure in the absorption cell was 0.458 Torr.

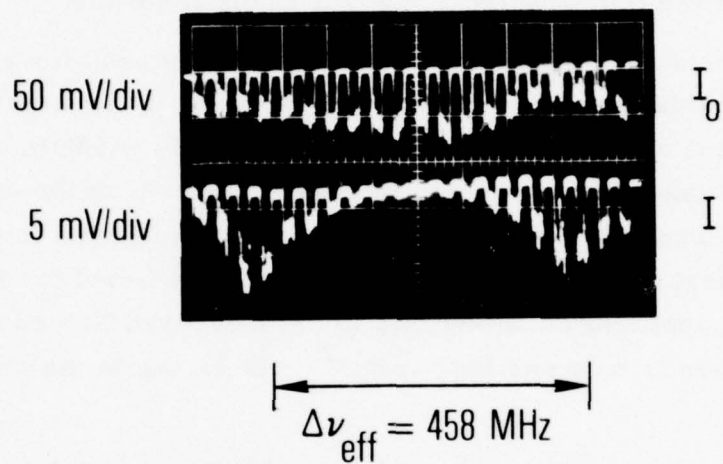


Fig. 8. Oscilloscope Record of Typical Intensity Scan of Absorption Line. Upper trace I_0 is laser intensity before absorption cell. Lower trace I is laser intensity after the absorption cell. Free spectral scanning range of probe laser = 458 MHz. Pressure $P = 0.458 \text{ Torr}$.

A nondimensional plot of the variation of the measured $\alpha/\alpha_0 = \ln(I/I_0)/\ln(I/I_0)_0$ as a function of the effective frequency ν_{eff} for $P_1(7)$ and three different pressures and free scanning ranges are shown in Fig. 9. The solid curve is the theoretically predicted Doppler profile, which has a FWHM of $\Delta\nu_D = 302$ MHz at the temperature $T = 297$ K of the absorber.

The agreement between experiment and theory is good for all three experiments, and this agreement can only be obtained if the empty laser cavity free spectral ranges of the three different cavity-medium configurations of the probe laser are corrected for mode pulling with the aid of Eq. (8). If this correction was not made, the experimentally measured line widths were 15 to 30% larger than the Doppler line widths predicted for 297 K. Since there are also no apparent discontinuities in the measured line shape, it was concluded that there is only one longitudinal mode lasing in the probe laser cavity.

The measured center-line absorption coefficient α_0 is shown as a function of pressure p for the three lines investigated in Fig. 10. The solid curves are straight lines of slope 1 in the log-log plot in Fig. 10, as should be the case for Doppler-broadened lines. At pressures above 7 Torr, the data begin to fall below the straight lines, indicating the onset of pressure broadening.

Values for $\alpha_0/P(\text{cm}^{-1})$, which were obtained by averaging over all experimental points for each of the three lines, and their standard deviations are given in Table 2. These experimental values can be compared with those numerically predicted and given in Table 1. The agreement between measured and calculated absorption coefficient α_0 is excellent for all three lines.

C. MEASUREMENTS OF ANOMALOUS REFRACTIVE INDEX

Figure 11a is a typical scan of the interferometer fringes. The horizontal axis represents the distance across the fringes; it is swept by the time base of the oscilloscope at 20 $\mu\text{sec}/\text{cm}$. The vertical axis, driven by the

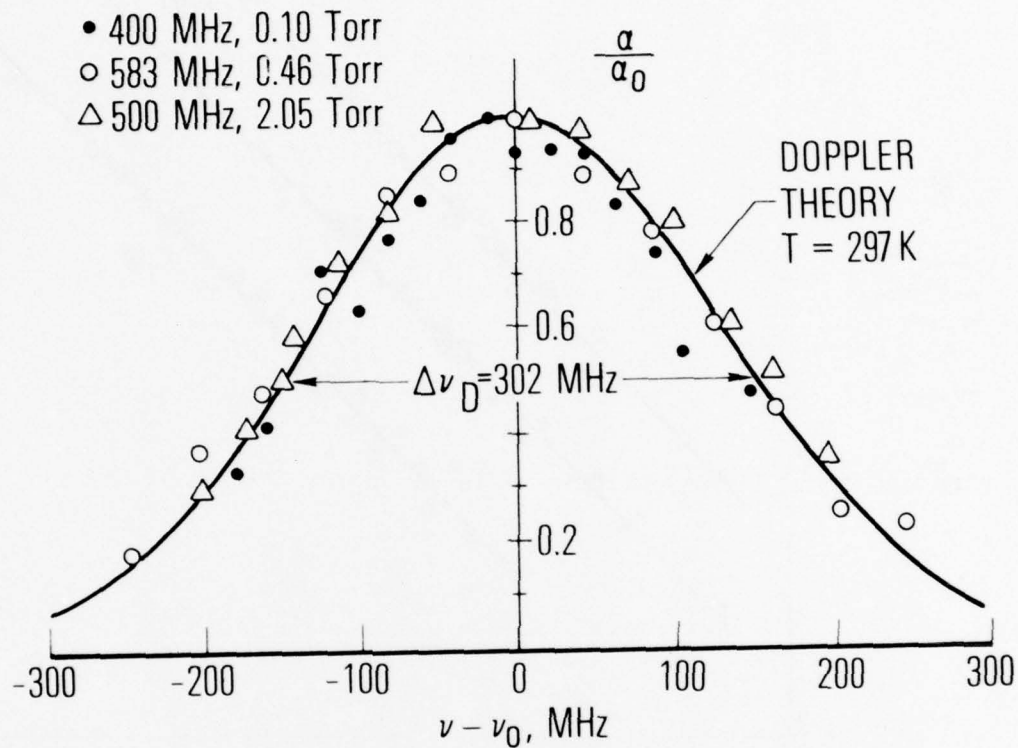


Fig. 9. Measured Absorption Line Profiles of $P_1(7)$ for Three Different Combinations of Gas Pressure and Laser Scanning Range. Solid curve is theoretically predicted Doppler profile for this line at $T = 297\text{ K}$. Note absence of sudden mode jumps.

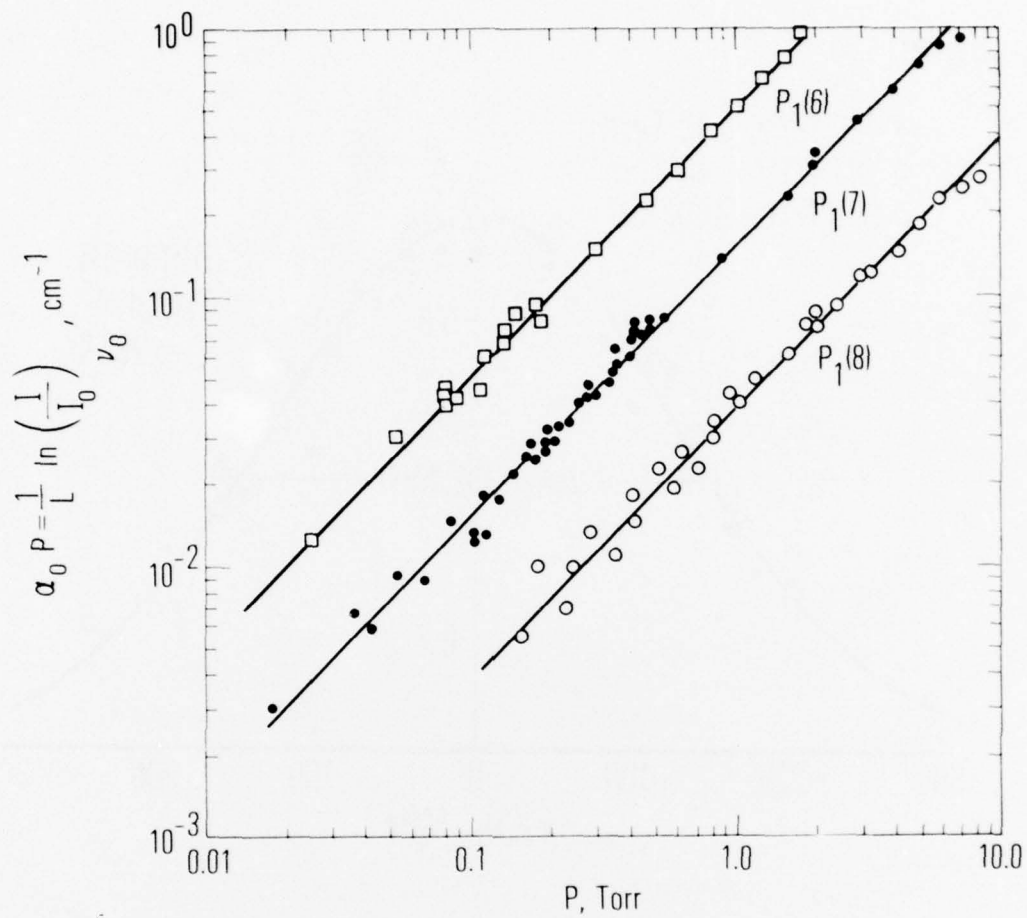
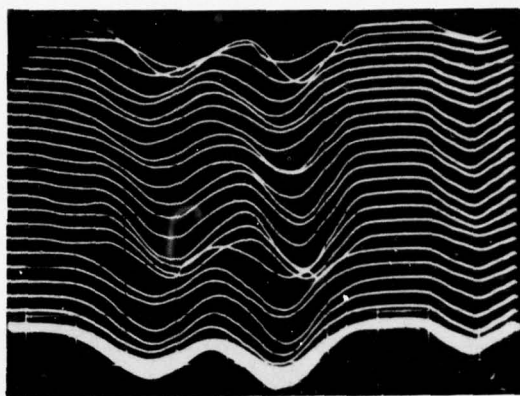
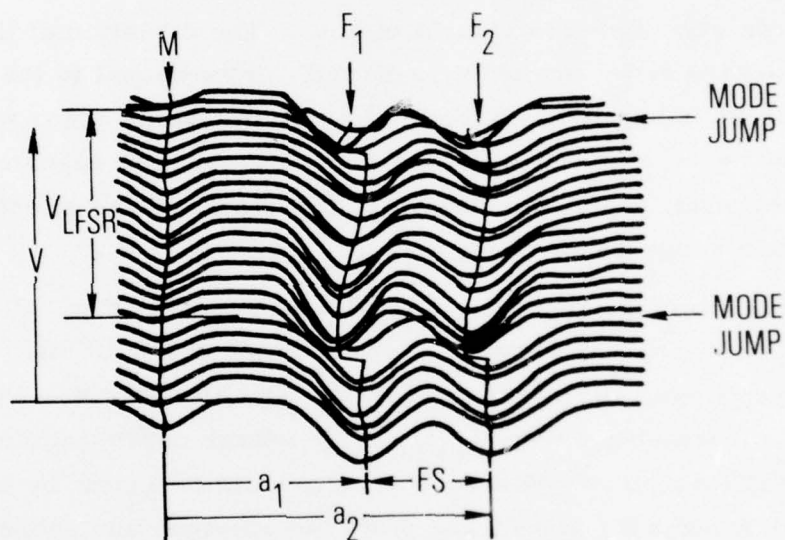


Fig. 10. Absorption of Three HF Ground-State Transitions Measured at Line Center as Functions of Gas Pressure (pure HF). Solid lines have slope of 1.



a.



b.

Fig. 11. Oscilloscope Trace of Typical Fringe Shift Measurement of $P_1(7)$. Gas pressure = 3.15 Torr. Short absorption cell. Effective scanning range LFSR = 551 MHz. (a) OSC2 record. (b) Tracing of record.

output of the high-voltage amplifier, is proportional to the PZT driver voltage, and, hence, to the frequency scan of the laser. Each fringe scan samples the fringe positions at one specific frequency. The vertical axis has a total time excursion of 100 msec. The gas pressure in the absorption cell was 0.215 Torr and the laser was tuned to the $P_1(7)$ line.

The oscilloscope trace is interpreted in Fig. 11b. The first signal excursion M is the time marker that serves as a trigger for the oscilloscope and as the reference point against which the fringe positions are measured. The fringes are F_1 and F_2 . Their distances from M are a_1 and a_2 . The fringe spacing is FS. The fringe displacement as a function of frequency caused by the changing refractive index is clearly visible. The deviation of the fringes from some arbitrary reference point is directly proportional to the refractive index. Two abrupt fringe jumps are visible. These jumps occur when a new mode enters the gain line of the laser and the scan is repeated. The time between the mode jumps corresponds, therefore, to the effective free spectral scanning range LFSR of the laser.

The evaluation of the record of Fig. 11b is shown in Fig. 12. The measured fringe shift $a - a_{CL}$, where a_{CL} is the center of the LFSR, is normalized with the fringe spacing FS to yield y . The abscissa x is the PZT voltage $V - V_{CL}$ normalized with V_{LFSR} , the voltage corresponding to the LFSR. The oscilloscope records were enlarged and evaluated by hand. Points taken from both fringes F_1 and F_2 and from the previous and subsequent scans were included in the evaluation. The maximum fringe shift is about 0.1 fringe spacings in either direction in this case. The maximum fringe jump Δy_{JU} and the slope at line center $(dy/dx)_0$ are also indicated. The reason for the offset of the actual line center from the center of the LFSR is a small detuning of the scanning cavity from the center of the laser line. Since all measurements are relative, this detuning has no influence on the measurements.

The effective scanning range in this case was 551 MHz, corresponding to a cavity of length $L = 25.7$ cm. With such a large scanning range, the two

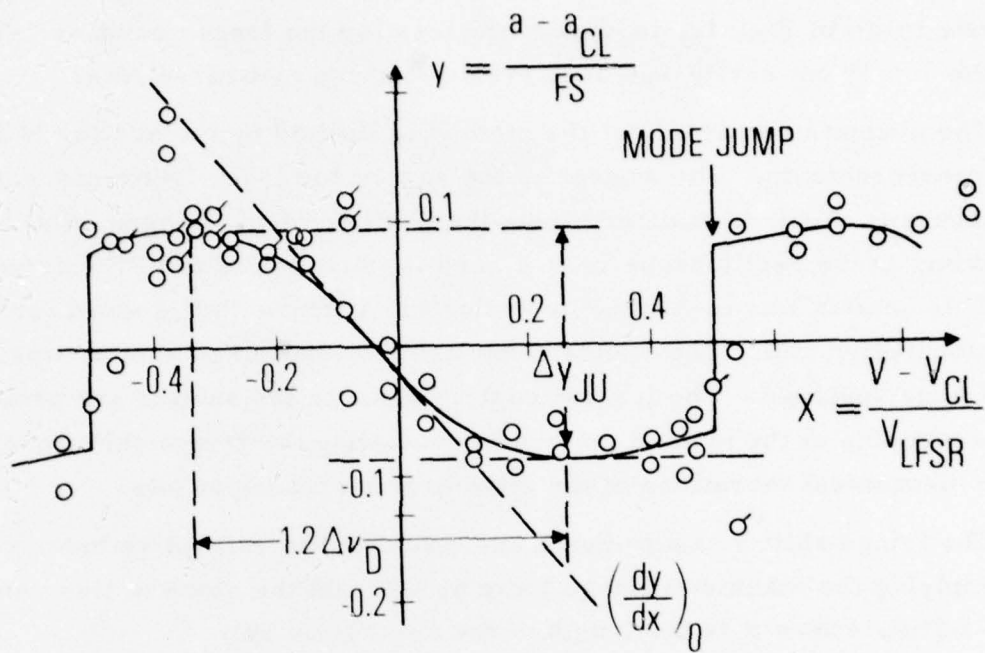


Fig. 12. Anomalous Dispersion Curve Derived from Experimental Record of Fig. 11

extrema of the anomalous dispersion curve, separated by $1.2 \Delta\nu_D = 362$ MHz, are clearly discernible, which is not the case for the longer laser cavities that have a smaller free spectral range. The scatter of the data points, which is relatively large in Fig. 12, is, however, less for the longer cavities. Therefore, the $L = 30$ cm cavity was used for most of the measurements.

The ultimate sensitivity of the method is limited by the scatter of the fringe measurements. The scatter is the sum of the laser frequency scatter, the inaccuracy involved in determining the position of the fringes, that is, the maxima in the oscilloscope record, and fluctuations of the PZT driver voltage. This scatter was measured by evaluating a fringe shift record for an empty absorption cell. The standard deviation of the fringe scatter was ± 0.01 fringe spacings. The largest contributions to the scatter are probably the inaccuracies of the manual method of evaluating the fringe-shift records and the mechanical vibrations of the interferometer components.

The fringe-shift measurements are converted to refractive index values by multiplying the maximum fringe jump by λ/\mathcal{L} and the slope at line center by λ/\mathcal{L} LFSR, where \mathcal{L} is the length of the absorption cell

$$\Delta(\eta - 1)_{JU} = \frac{\lambda}{\mathcal{L}} \Delta y_{JU} \quad , \quad \left(\frac{d\eta}{d\nu}\right)_{\nu_0} = \frac{\lambda}{\mathcal{L} \text{ LFSR}} \left(\frac{dy}{dx}\right)_0$$

The measured values for $\Delta(\eta - 1)_{JU}$ and $(d\eta/d\nu)_{\nu_0}$ plotted as functions of pressure for the three investigated HF absorption lines are given in Figs. 13 and 14.

The least squares curves through the data are straight lines of Slope 1 in the log-log planes in Figs. 13 and 14. The two quantities depend, therefore, linearly on pressure as predicted by theory. The averaged values and standard deviations of $(1/P)\Delta(\eta - 1)_{JU}$ and $(1/P)(d\eta/d\nu)_{\nu_0}$ are also given in Table 2 for each of the three lines, where they can be compared with their numerically predicted values given in Table 1. The measured values are slightly larger

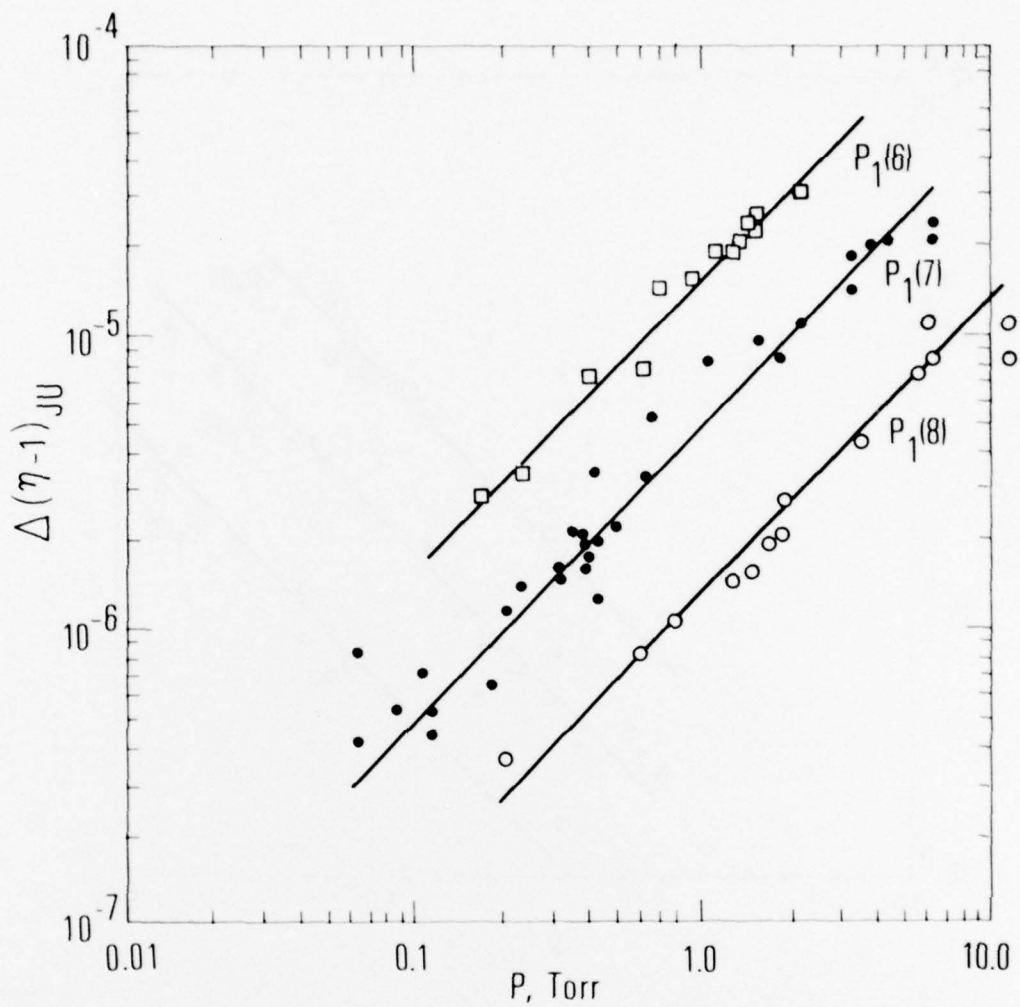


Fig. 13. Maximum Jump of Refractive Index Measured as Function of Pressure in Absorption Cell. Maximum jump is equal to sum of absolute magnitude of two extrema of dispersion curve. Lines through data have slope of 1.

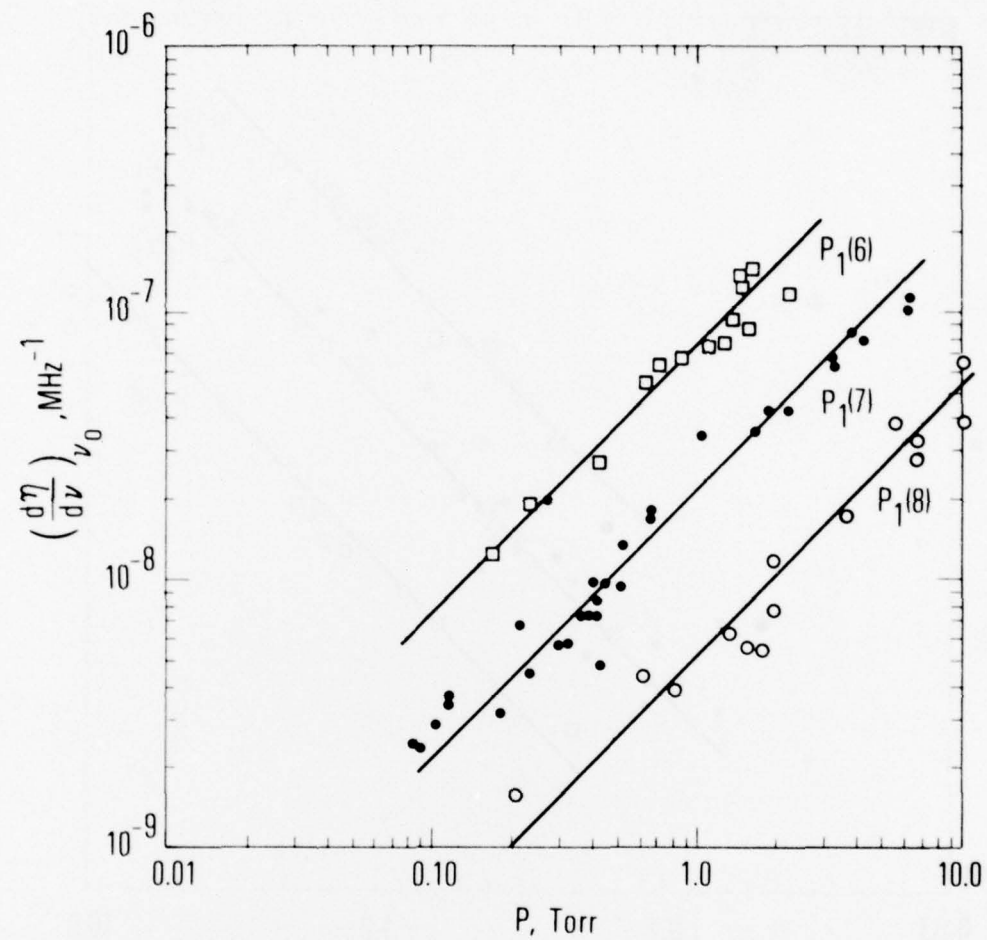


Fig. 14. Slope of Anomalous Dispersion Curve at Line Center Measured as Function of Pressure in Absorption Cell. Lines through data have slope of 1.

than the theoretical for all quantities [except the slope of the dispersion curve of $P_1(8)$], which may be the result of the small, but nonzero, contributions from the neighboring lines that would be seen by the laser beam at the place of the line under investigation. This contribution was neglected in the theory. Nevertheless, the theoretically predicted values are well within the experimental scatter for all measured data.

V. CONCLUSIONS

An interferometric technique with direct readout of the fringes in the infrared was developed and successfully used to measure the anomalous dispersion of three ground-state transitions of HF in absorption.

A small line-tunable cw HF laser was used as a monochromatic source to illuminate a Mach-Zehnder interferometer that contained the HF absorption cell. The cavity of the HF laser was scanned across the laser gain line by a piezoelectrically driven mirror and therefore permitted the investigation of the dispersion of a corresponding absorption line across a large part of its profile. The effective free scanning range of the laser, corrected for mode pulling, could be made as large as 551 MHz. The PZT mirror was driven by a sawtooth voltage with a sweep duration of 100 msec.

The design of the Mach-Zehnder interferometer was conventional. The absorption cell occupied one arm of the interferometer. The fringes produced by the interferometer were scanned with the aid of a three-face mirror rotating at 2800 rpm and a single-point In-Sb detector. The rotating mirror used in the present experiments permitted the full fringe pattern to be scanned in 150 μ sec with a repetition rate of 140 Hz. The fringes were scanned 15 to 20 times during one frequency scan of the laser. The entire set of fringe samplings during one frequency scan was recorded on one oscilloscope face, and the fringe shifts, which are proportional to the index of refraction, were measured from such a record. This procedure reduced the inaccuracies introduced into the measurements by the high-frequency jitter of the laser cavity, leaving only a slow frequency drift that was corrected for by manually adjusting the bias level of the PZT.

The objective is to use this technique in measurements of the anomalous dispersion of the saturated gain lines in an HF laser, the gain coefficient of which may be small and varying in time; therefore, it is of interest to estimate the limitations of the method.

The time resolution of 100 msec of the fringe shift measurements is at present limited by the rotating mirror scanner or by the number of fringe samplings desired during one frequency scan, or both. A minimum of ten samplings is needed to make a reasonable reconstruction of a complete anomalous dispersion curve. The sweep rate of the PZT and, hence, the frequency scan can be reduced to 10 msec, the limit of the transducer. A rotating mirror with an effective scan frequency of 1000 Hz is needed to produce ten fringe scans during 10 msec. With a six-faceted mirror, a 10,000-rpm motor is required. Mirrors rotating at speeds faster than this are commercially available. The time resolution of the fringe measurements will then be limited by the PZT to 10 msec or 100 Hz. The same limit applies to time-resolved measurements of the gain profile.

The sensitivity of the interferometer measurements of the dispersion is ultimately limited by the jitter of the positions of the individual fringes with respect to the reference marker signal. This jitter was measured by observing the fringes produced by an empty absorption cell. After the usual manual evaluation of the oscilloscope record, a standard deviation of the fringe positions from zero displacement of $\Delta y_{\text{jitt}} = \pm 0.01$ fringe spacings was found. This measurement includes the contributions from all sources to the jitter: (1) mechanical, such as vibrations of the interferometer components, the windows of the absorption cell, the rotating mirror, and the detector in the fringe readout; (2) optical, primarily density fluctuations in the air inside the interferometer and frequency fluctuations of the scanning laser cavity; and also (3) errors and inaccuracies in locating and measuring the positions of the maxima or minima of the fringe records. Nevertheless, the measured absolute scatter of $2/100$ of a wave at $2.7 \mu\text{m}$ is five times better than that quoted for measurements with a Mach-Zehnder interferometer in the visible.¹¹ The reason is, of course, that with the jitter being primarily the result of

¹¹R. W. Ladenburg and D. Bershader, "Interferometry," in Princeton Series on High Speed Aerodynamics and Jet Propulsion, Volume IX, Physical Measurements in Gas Dynamics and Combustion, R. W. Ladenburg, ed., Princeton University Press, Princeton, N. J. (1954).

mechanical excursions of the interferometer parts, the five times longer wave length used results in a corresponding improvement in the measurements compared to those in the visible.

This sensitivity limit can also be expressed in terms of a centerline small-signal-gain coefficient of an amplifier mechanism. If the line is assumed to be unsaturated, or at least uniformly saturated, the centerline small-signal-gain coefficient g_0 and the maximum jump of the anomalous refractive index $\Delta(\eta - 1)_{JU}$ associated with that transition are related by

$$\Delta(\eta - 1)_{JU} = \frac{0.5381 \lambda_0}{\pi^{3/2}} g_0 \quad (12)$$

For a length \mathcal{L} of the gain medium, this refractive index change is related to the absolute magnitude of the smallest measurable fringe shift Δy_{MIN} by

$$\Delta y_{MIN} = \frac{\mathcal{L}}{\lambda_0} \Delta(\eta - 1)_{JU} \geq 2 |\Delta y_{jitt}| \quad (13)$$

By the combination of Eq. (12) and (13), an expression results for g_{0MIN} , the smallest gain coefficient for which refractive index measurements can be made

$$g_{0MIN} \geq \frac{\pi^{3/2}}{0.5382 \mathcal{L}} 2 |\Delta y_{jitt}|$$

Such measurements in the 17-cm medium of The Aerospace Corporation supersonic HF laser are planned. For this device, g_{0MIN} will be

$$g_{0MIN} \geq 4.3 \times 10^{-3} \text{ cm}^{-1}$$

The zero power gain in this laser device is of the order of 10%/cm, and this method, therefore, should be sufficiently sensitive for measurements of the

refractive index in this medium. In fact, the method should permit measurements even on lines that are weakly saturated.

In this assessment, contributions to the fringe scatter by statistical density fluctuations of the absorbing or gain medium are not considered. No reliable measurements of the magnitude of the density fluctuations in a supersonic diffusion laser exist by which the size of this disturbance on the fringes can be predicted. Note that this method would also lend itself to a very sensitive measurement of such density fluctuations at the actual wavelength at which the laser medium is being utilized.

LABORATORY OPERATIONS

The Laboratory Operations of The Aerospace Corporation is conducting experimental and theoretical investigations necessary for the evaluation and application of scientific advances to new military concepts and systems. Versatility and flexibility have been developed to a high degree by the laboratory personnel in dealing with the many problems encountered in the nation's rapidly developing space and missile systems. Expertise in the latest scientific developments is vital to the accomplishment of tasks related to these problems. The laboratories that contribute to this research are:

Aerophysics Laboratory: Launch and reentry aerodynamics, heat transfer, reentry physics, chemical kinetics, structural mechanics, flight dynamics, atmospheric pollution, and high-power gas lasers.

Chemistry and Physics Laboratory: Atmospheric reactions and atmospheric optics, chemical reactions in polluted atmospheres, chemical reactions of excited species in rocket plumes, chemical thermodynamics, plasma and laser-induced reactions, laser chemistry, propulsion chemistry, space vacuum and radiation effects on materials, lubrication and surface phenomena, photo-sensitive materials and sensors, high precision laser ranging, and the application of physics and chemistry to problems of law enforcement and biomedicine.

Electronics Research Laboratory: Electromagnetic theory, devices, and propagation phenomena, including plasma electromagnetics; quantum electronics, lasers, and electro-optics; communication sciences, applied electronics, semi-conducting, superconducting, and crystal device physics, optical and acoustical imaging; atmospheric pollution; millimeter wave and far-infrared technology.

Materials Sciences Laboratory: Development of new materials; metal matrix composites and new forms of carbon; test and evaluation of graphite and ceramics in reentry; spacecraft materials and electronic components in nuclear weapons environment; application of fracture mechanics to stress corrosion and fatigue-induced fractures in structural metals.

Space Sciences Laboratory: Atmospheric and ionospheric physics, radiation from the atmosphere, density and composition of the atmosphere, aurorae and airglow; magnetospheric physics, cosmic rays, generation and propagation of plasma waves in the magnetosphere; solar physics, studies of solar magnetic fields; space astronomy, x-ray astronomy; the effects of nuclear explosions, magnetic storms, and solar activity on the earth's atmosphere, ionosphere, and magnetosphere; the effects of optical, electromagnetic, and particulate radiations in space on space systems.

THE AEROSPACE CORPORATION
El Segundo, California